

# Electronic Supplementary Material

*for the article*

Origin and evolution of gold-bearing fluids in a carbon-rich  
sedimentary basin: a case study of the Algamarca  
epithermal gold-silver-copper deposit, northern Peru

R. Galdos, J. Vallance, P. Baby, S. Salvi, M. Schirra, G. Velasquez, W. Viveen,  
R. Soto, and G.S. Pokrovski

**This file contains:**

Figures A1 to A6

Tables A1 to A7

List of cited references

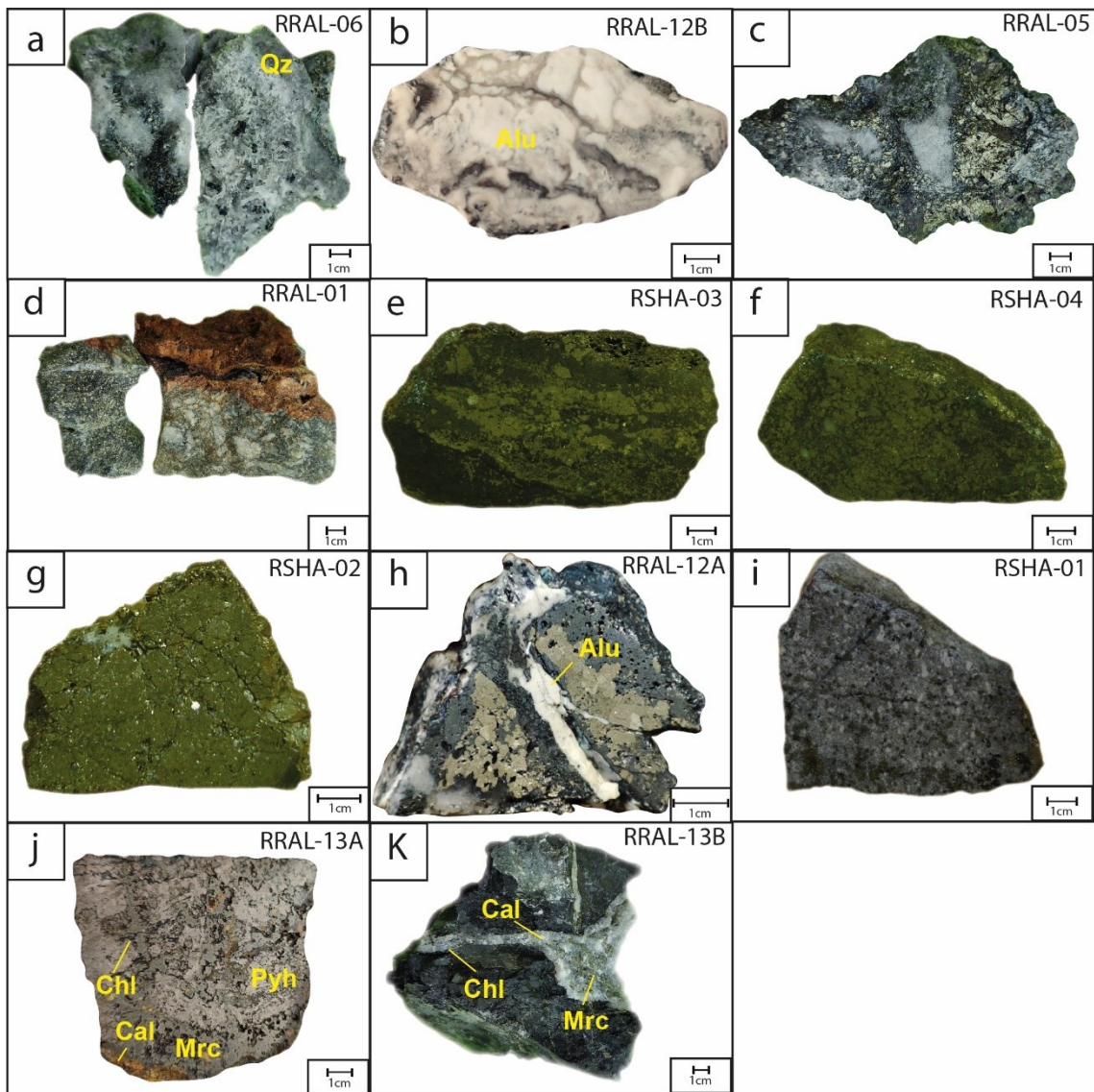


Fig. A1. Representative hand specimens, labeled by their sample numbers (displayed in the upper right corner). (a) Centimetric hydrothermal quartz crystals from the Concepción vein showing a crustiform texture. (b) Colloform alunite from Lucy vein. (c) Typical mineral assembles of the Lucy vein matrix formed by pyrite-quartz-tenantite-tetrahedrite accompanied by clasts of quartzite from the Chimú Formation. (d) Hydrothermal breccia from the Cholque vein with clasts of quartzite and matrix of quartz and pyrite, partially oxidized. (e) Typical ore mineral assemblage of tenantite-pyrite-chalcopyrite from the Alisos vein. (f) Typical ore mineral assemblage of chalcopyrite-quartz-tetrahedrite-pyrite from the San Blas vein. (g) Massive pyrite, with minor baryte (white) from the San Blas vein. (h) Pyrite and tenantite-tetrahedrite from stage B, both crosscut by an alunite vein from stage C, Lucy vein. (i) Pre-ore diorite intrusive rock with abundant disseminated pyrite. (j) Massive pyrrhotite was replaced by marcasite. Chlorite and calcite are mainly in the contact between pyrrhotite and marcasite. (k) Veins of calcite-marcasite with narrow chlorite halo. In all figures, mineral abbreviations follow Warr (2021).

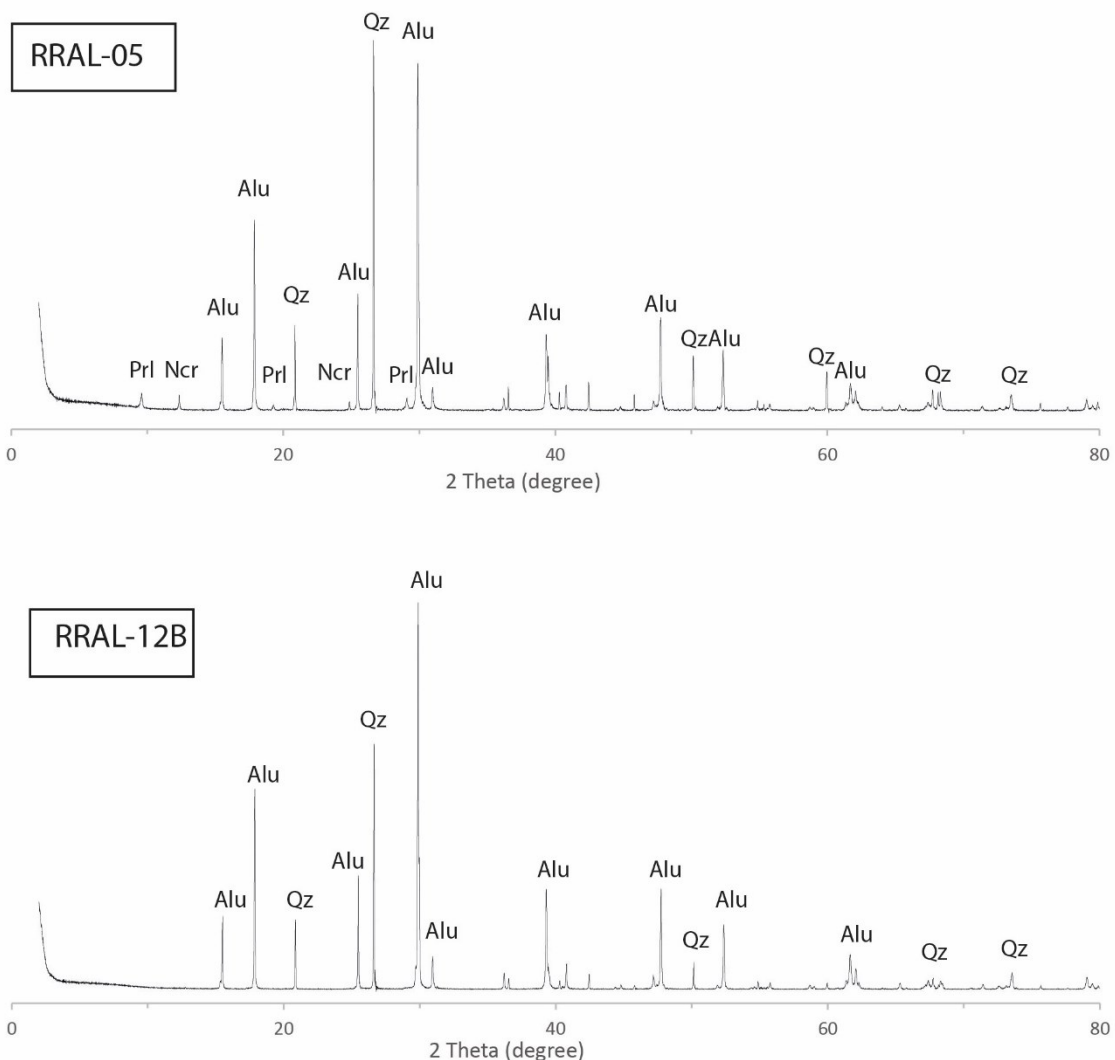


Fig. A2. XRD patterns of gangue minerals from Stage C for two indicated samples.

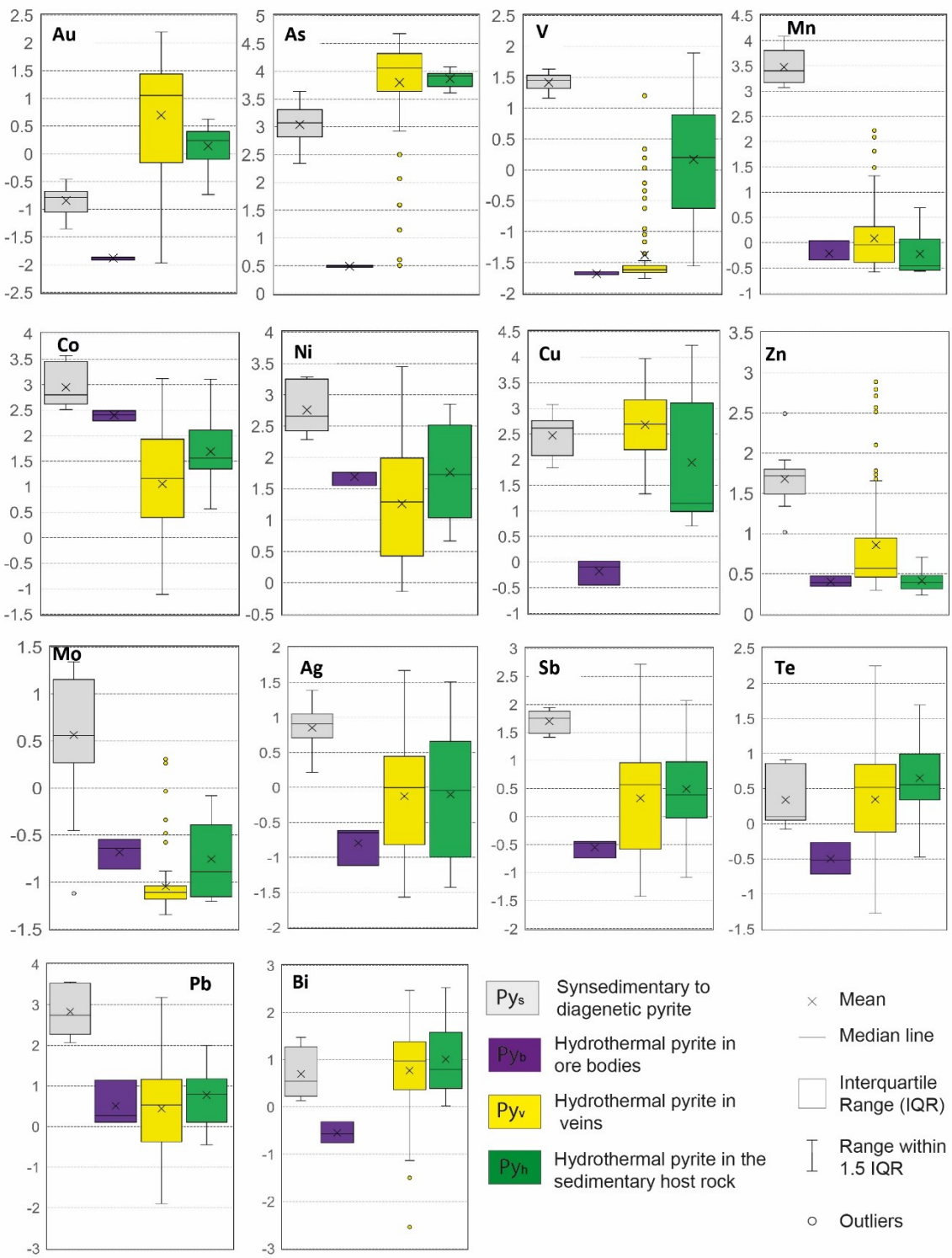


Fig. A3. Box plot comparison of the content in  $\log_{10}$  (ppm) of elements analyzed by LA-ICPMS in the different pyrite types from the Algamarca deposit.

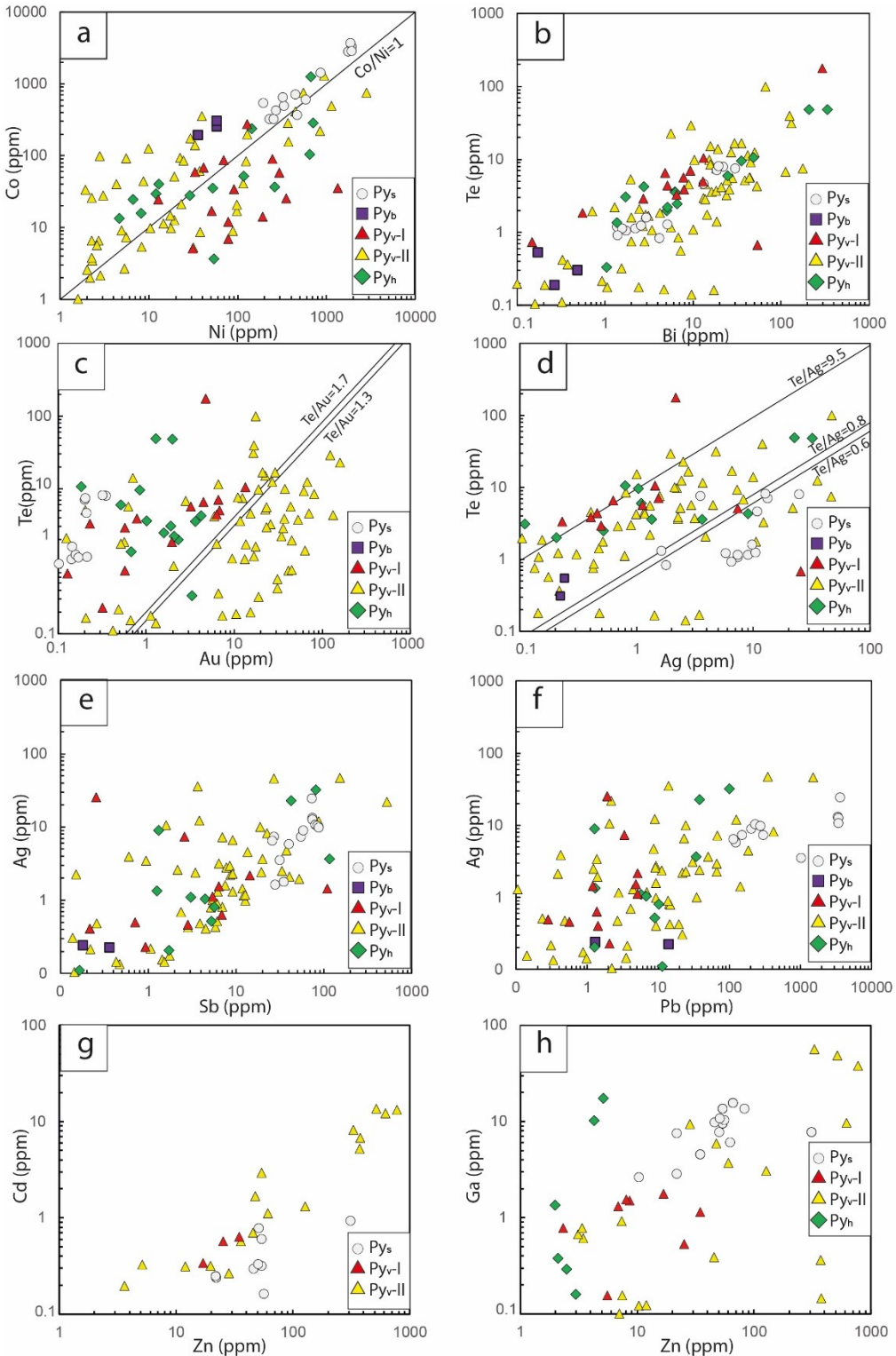


Fig. A4. Scatter diagrams of traces elements in all the types of pyrite from the Algamarca deposit. Abbreviations for pyrite types are the same as in Table 2. (a) Co vs. Ni. (b) Te vs. Bi. (c) Te vs. Au. (d) Te vs. Ag. (e) Ag vs. Sb. (f) Ag vs. Pb. (g) Cd vs. Zn. (h) Ga vs. Zn. The lines in Fig. A4c, d represents the ratios of common Au-Ag tellurides: calaverite ( $\text{Te}/\text{Au} = 1.3$ ), petzite ( $\text{Te}/\text{Au} = 1.3$  and  $\text{Te}/\text{Ag} = 0.8$ ), sylvanite ( $\text{Te}/\text{Au} = 1.7$  and  $\text{Te}/\text{Ag} = 9.5$ ), and hessite ( $\text{Te}/\text{Ag} = 0.6$ ).

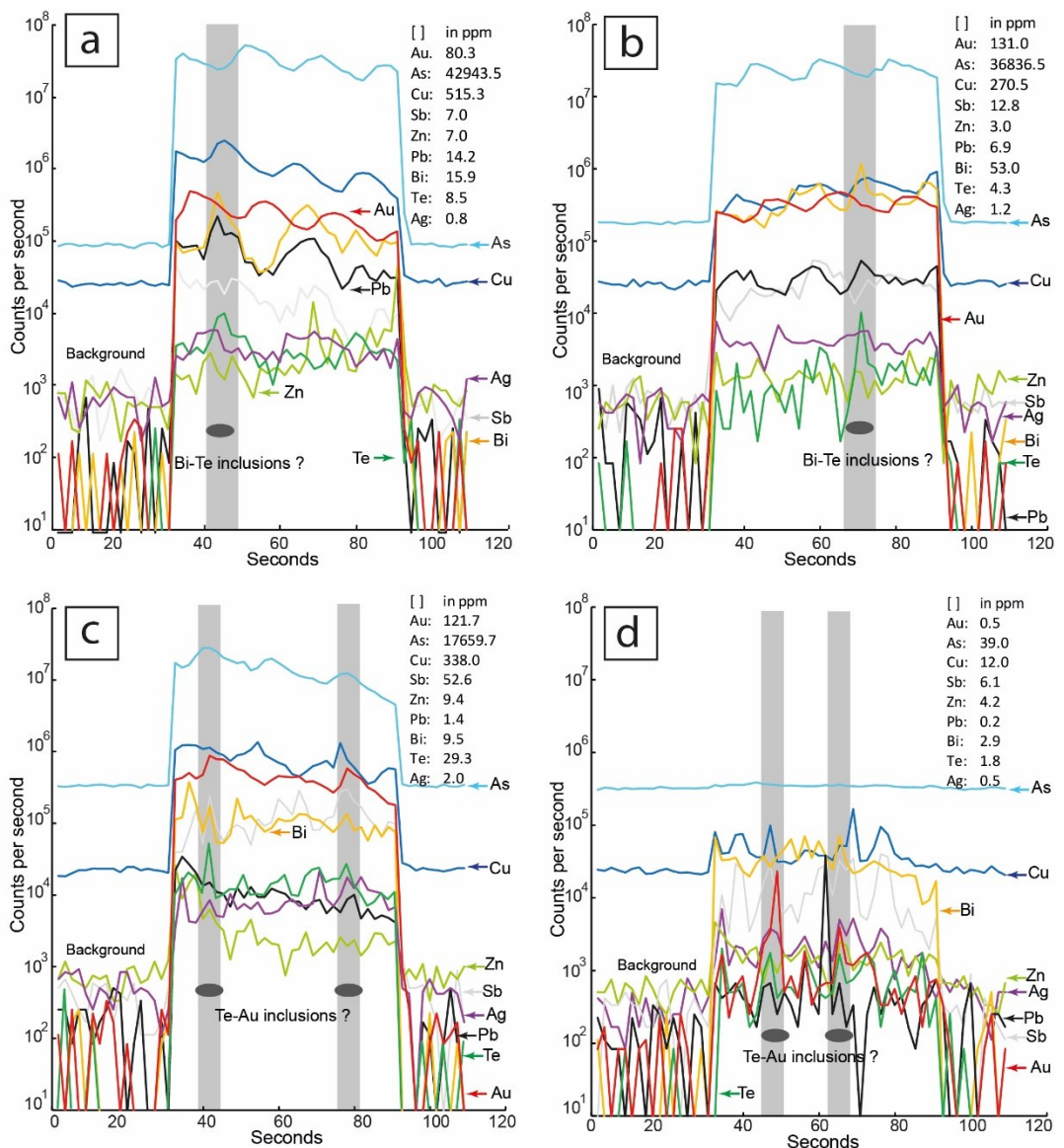


Fig. A5. LA-ICPMS signals for selected elements obtained from spot analyses of hydrothermal pyrites in veins. The spiky peaks highlighted in gray indicate the presence of inclusions. (a) Py<sub>v</sub>-II<sub>b</sub> from the Concepción vein, (b) Py<sub>v</sub>-II<sub>e</sub> from the Lucy vein, (c) Py<sub>v</sub>-II<sub>b</sub> from the San Blas vein, and (d) Py<sub>v</sub>-II<sub>c</sub> from the San Blas vein.

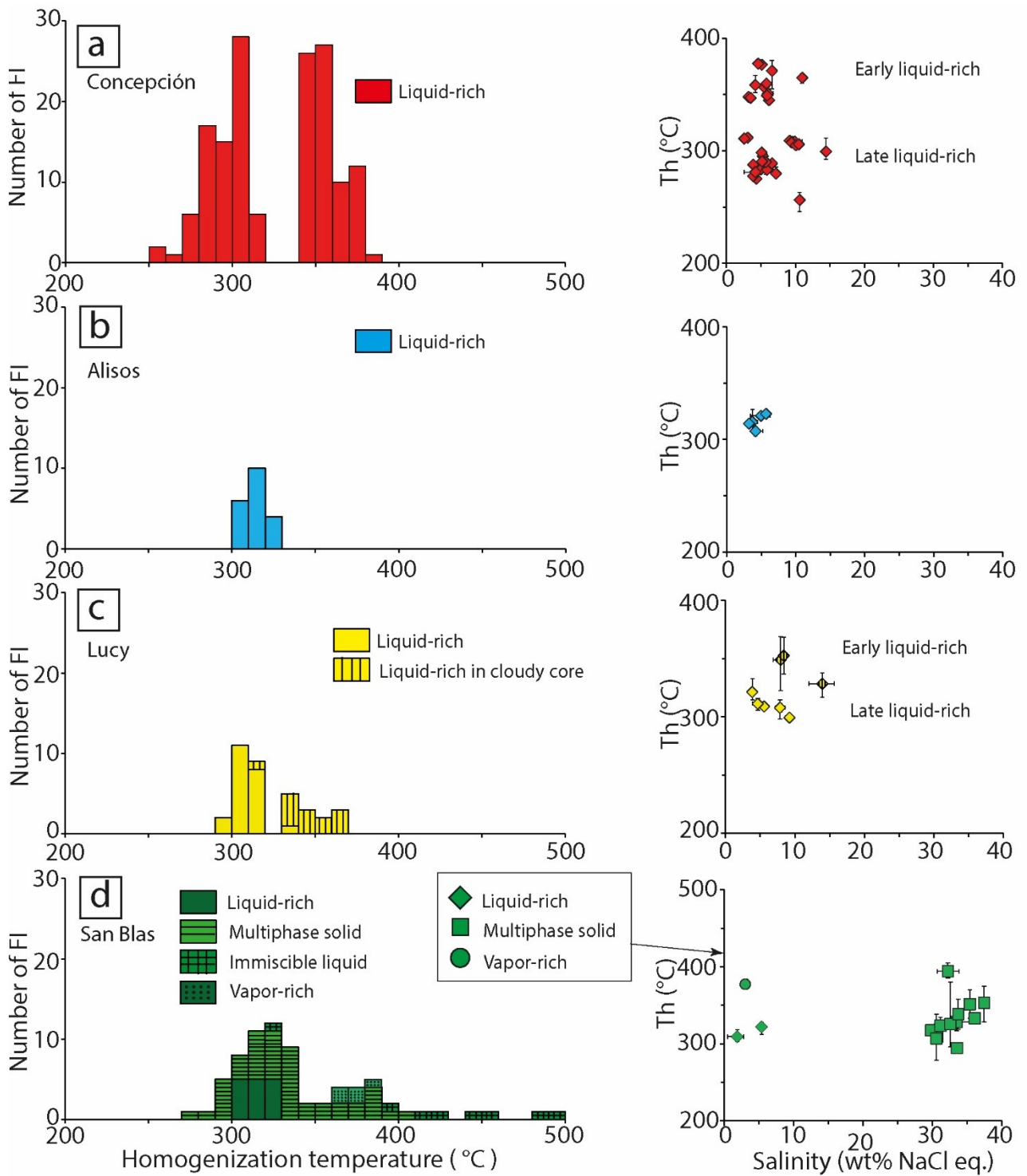


Fig. A6. Frequency vs. temperature of homogenization and temperature of homogenization vs. salinity for the Algamarca veins. The error bars correspond to the minimum and maximum value for each fluid inclusion assemblage.

Table A1. Representative EPMA analyses of different hydrothermal pyrites types. Including the chemical composition and structural formulas.

Stage	Stage A		Stage B										d.l.		
	Pyrite in veins		Pyrite in veins												
Mineral	Py <sub>v</sub> -I		Py <sub>v</sub> -II										Py <sub>h</sub>		
	Py <sub>v</sub> -I		Py <sub>v</sub> -II <sub>a</sub>										core	rim	
Sample	RSHA-04	RSHA-04	RRAL-06	RRAL-06	RRAL-06	RSHA-02	RRAL-06	RRAL-05	RRAL-05	RRAL-06	RSHA-01	RRAL-06	RRAL-01A	RRAL-01A	
#	47	3	8	27	25	74	5	10							
As (wt%)	0.22	1.15	0.15	0.15	3.77	2.58	2.02	b.d.l.	0.53	2.77	0.12	2.56	0.16	1.12	0.06
S	53.54	52.46	53.17	53.17	50.68	51.63	52.11	53.79	53.99	51.67	53.14	51.78	53.88	52.63	0.06
Fe	47.67	47.52	47.13	47.13	46.65	46.46	46.69	47.13	47.88	46.83	47.59	46.68	47.34	47.19	0.07
Sb	b.d.l.	b.d.l.	b.d.l.	b.d.l.	b.d.l.	b.d.l.	b.d.l.	b.d.l.	b.d.l.	b.d.l.	b.d.l.	b.d.l.	b.d.l.	b.d.l.	0.03
Cu	n.m.	n.m.	n.m.	n.m.	n.m.	b.d.l.	n.m.	n.m.	n.m.						
Total	101.45	101.14	100.46	100.46	101.11	100.67	100.82	100.93	102.4	101.28	100.85	101.02	101.40	100.94	
As (apfu)	0.00	0.02	0.00	0.00	0.06	0.04	0.03	0.00	0.01	0.04	0.00	0.04	0.00	0.02	
S	1.98	1.96	1.99	1.99	1.92	1.95	1.96	2.00	1.98	1.94	1.98	1.95	1.99	1.97	
Fe	1.02	1.02	1.01	1.01	1.02	1.01	1.01	1.00	1.01	1.01	1.02	1.01	1.00	1.01	
Total	3.00	3.00	3.00	3.00	3.00	3.00	3.00	3.00	3.00	3.00	3.00	3.00	3.00	3.00	

# = number of electron microprobe analyses, d.l. = detection limit in wt%, b.d.l.= below detection limit, n.m. = not measured. Abbreviations for pyrite types are the same as in Table 2.

**Table A2.** Representative EPMA analyses (in wt% and atomic units) of sedimentary pyrite and other indicated sulfide minerals from veins and ore bodies.

Mineral Sample #	Sedimentary to diagenetic pyrite				Sulfides in ore bodies						Sulfide in veins from Stage B				d.l. 12	
	Py <sub>s</sub> RRAL-03 12		Py <sub>b</sub> RRAL-13A 10		Po RRAL-13A 4		Mrc RRAL-13A 10		Ttr RRAL-13A 23		Tnt RSHA-04 6		Ccp RSHA-02 RSHA-04 12			
	RRAL-03	RRAL-03	RRAL-13A	RRAL-13A	RRAL-13A	RRAL-13A	RSHA-04	RSHA-04	RSHA-03	RSHA-02	RSHA-04	RSHA-04	RSHA-04	RSHA-04		
As (wt%)	0.08	0.22	b.d.l.	b.d.l.	b.d.l.	b.d.l.	b.d.l.	b.d.l.	1.73	2.91	18.67	20.40	b.d.l.	b.d.l.	0.06	
S	53.34	51.94	52.6	53.03	39.05	39.18	53.05	52.5	25.21	26.04	28.16	28.43	34.65	34.85	0.06	
Fe	47.48	46.81	47.72	47.62	61.72	61.12	47.7	47.25	5.12	5.45	6.19	8.29	30.27	30.48	0.07	
Sb	b.d.l.	b.d.l.	b.d.l.	b.d.l.	b.d.l.	b.d.l.	b.d.l.	b.d.l.	26.22	24.74	2.35	0.79	b.d.l.	b.d.l.	0.03	
Cu	n.m.	n.m.	n.m.	n.m.	n.m.	n.m.	n.m.	n.m.	38.12	37.93	43.75	42.42	34.80	34.70	0.05	
Ag	n.m.	n.m.	n.m.	n.m.	n.m.	n.m.	n.m.	n.m.	1.35	1.58	b.d.l.	b.d.l.	b.d.l.	b.d.l.	0.2	
Zn	n.m.	n.m.	n.m.	n.m.	n.m.	n.m.	n.m.	n.m.	1.73	1.65	1.05	0.32	b.d.l.	b.d.l.	0.2	
Bi	n.m.	n.m.	n.m.	n.m.	n.m.	n.m.	n.m.	n.m.	0.3	b.d.l.	b.d.l.	b.d.l.	b.d.l.	b.d.l.	0.3	
Total	100.9	98.98	100.35	100.66	100.77	100.3	100.75	99.75	99.80	100.30	100.17	100.65	99.72	100.03		
As (apfu)	0.00	0.00	0.00	0.00	0.00	0.00	0.00	0.00	0.38	0.64	3.67	3.98	0.00	0.00		
S	1.98	1.98	1.97	1.98	1.10	1.12	1.94	1.94	12.89	13.27	12.93	12.96	1.98	1.99		
Fe	1.02	1.02	1.03	1.02	1.00	1.00	1.00	1.00	1.50	1.59	1.63	2.17	0.99	1.00		
Sb									3.53	3.32	0.28	0.09	1.01	1.00		
Cu									9.83	9.75	10.13	9.76	0.00	0.00		
Ag									0.21	0.24	0.00	0.00	0.00	0.00		
Zn									0.43	0.41	0.24	0.07	0.00	0.00		
Bi									0.03	0.00	0.00	0.00	0.00	0.00		
Total	3.00	3.00	3.00	3.00	2.10	2.12	2.94	2.94	28.80	29.23	28.88	29.04	3.98	3.99		

# = number of electron microprobe analyses, d.l. = detection limit in wt%, b.d.l.= below detection limit, n.m. = not measured. Abbreviations for minerals follow Warr (2021) and for pyrite types are the same as in Table 2



**Table A4.** Pearson correlation coefficients for all bivariate trace element combinations in hydrothermal pyrite from the Algararca veins (Py<sub>v</sub>). Weak (light gray), moderate (medium gray) and high correlation (dark gray) are high.

	Au	As	V	Mn	Co	Ni	Cu	Zn	Ga	Se	Mo	Ag	Cd	In	Sn	Sb	Te	Pb	Bi
Au	1																		
As	0,6	1																	
V	-0,1	0,0	1																
Mn	-0,1	-0,1	0,0	1															
Co	0,0	0,1	0,0	-0,1	1														
Ni	-0,1	-0,1	0,0	0,0	0,6	1													
Cu	-0,1	-0,2	0,0	0,1	0,2	0,2	1												
Zn	-0,1	-0,1	0,0	0,0	-0,1	-0,1	0,2	1											
Ga	-0,1	-0,1	0,0	0,0	-0,1	-0,1	0,1	0,7	1										
Se	0,0	-0,2	-0,2	0,3	0,0	0,0	0,2	0,0	0,0	1									
Mo	-0,1	-0,1	0,6	-0,1	0,2	0,2	0,4	0,0	0,0	-0,2	1								
Ag	-0,1	-0,1	-0,1	0,1	0,0	0,0	0,4	0,3	0,0	0,3	0,0	1							
Cd	-0,1	-0,1	0,0	0,0	-0,1	-0,1	0,2	1,0	0,8	0,0	0,0	0,3	1						
In	-0,1	-0,1	0,0	0,1	-0,1	0,0	0,1	0,8	0,9	-0,1	0,0	0,0	0,8	1					
Sn	-0,1	-0,1	0,0	0,0	-0,1	0,0	0,1	0,8	0,8	0,0	0,0	0,0	0,9	1,0	1				
Sb	0,0	-0,1	0,0	0,1	-0,1	-0,1	0,5	0,4	0,0	0,2	-0,1	0,4	0,3	0,0	0,0	1			
Te	0,1	0,0	-0,1	0,1	0,0	-0,1	0,2	0,1	0,1	0,5	-0,1	0,3	0,1	0,0	0,1	0,2	1		
Pb	-0,1	-0,1	0,0	0,0	-0,1	-0,1	0,0	0,3	0,0	0,1	0,0	0,6	0,2	0,0	0,0	0,1	0,1	1	
Bi	0,0	0,0	-0,1	0,2	-0,1	0,1	0,3	0,1	0,2	-0,1	0,4	0,2	0,1	0,1	0,1	0,7	0,5	1	

Table A5. Microthermometric results of immiscible-liquid fluid inclusion assemblages (FIAs) in quartz of stage A from the San Blas vein. For each microthermometric parameter, the average values are given, while the number of analyzed fluid inclusions are in brackets.

Sample	Type	Th (°C)	Tm <sub>(CO<sub>2</sub>)</sub> (°C)	Tm <sub>(clath)</sub> (°C)	Th <sub>(CO<sub>2</sub>)</sub> (°C)
RSHA-04	C	>370	(5)	-66.8 ± 1.3 (3)	10.6 ± 2.1 (3)
RSHA-04	I	498	(1)	-66.2 (1)	10.1 (1)
RSHA-04	I	327	(1)	-65.8 (1)	10.3 (1)
RSHA-04	C	404 ± 17 (2)	-65.9 ± 1.1 (3)	9.1 ± 4.3 (2)	30.9 ± 0.4 (3)
RSHA-04	C	444 ± 25 (3)	-66.5 ± 0.5 (3)	9.8 ± 1.7 (3)	31.0 ± 0.1 (4)

Th = homogenization temperature, Tm<sub>(CO<sub>2</sub>)</sub> = melting temperature of solid CO<sub>2</sub>, Tm<sub>(clath)</sub> = melting temperature of clathrate, Th<sub>(CO<sub>2</sub>)</sub> = homogenization temperature of CO<sub>2</sub>, C = cluster, I = isolated.



Table A.7. Relevant Raman peak parameters and estimated temperatures from Raman spectra of carbonaceous material at the Algamarca deposit.

Sample	Analysis	Position (cm <sup>-1</sup> )					Area					FWHM	Area ratio	Estimated temperature (°C)	
		D4	D1	D3	G	D2	D4	D1	D3	G	D2				
RRAL-07	1	1215	1338	1521	1593	1610	58118	323058	51090	110599	40040	83	0.65	300	348
	2	1230	1338	1516	1593	1611	257913	810020	230738	363517	22683	86	0.63	293	323
RRAL-14A	1	1207	1333	1506	1593	1603	141804	718590	177509	273185	102037	109	0.61	243	291
	2	1205	1332	1507	1593	1603	275069	1058620	259769	456584	75651	114	0.63	233	315
	3	1202	1331	1508	1593	1603	233581	1072050	261730	452602	78045	114	0.62	232	308
	4	1207	1333	1506	1593	1604	105506	411466	94436	133517	87863	109	0.62	245	306
RRAL-14B	1	1204	1330	1511	1593	1603	251648	1225450	364442	537825	56424	113	0.61	234	288
	2	1205	1331	1511	1593	1603	296607	1040610	293744	458089	44465	114	0.63	232	314

Notes: FWHM = half width at half maximum, RA1 =  $(D1 + D4)/(D1 + D2 + D3 + D4 + G)$  area ratio, Tw = temperature estimated using the D1 width (FWHM) after Kouketsu et al. (2014), Ta = temperature estimated using the area ratio RA1 after Lahfid et al. (2010).

## **References cited**

- Kouketsu, Y., Mizukami, T., Mori, H., Endo, S., Aoya, M., Hara, H., Nakamura, D., Wallis, S., 2014. A new approach to develop the Raman carbonaceous material geothermometer for low-grade metamorphism using peak width. *Island Arc* 23, 33–50.
- Lahfid, A., Beyssac, O., Deville, E., Negro, F., Chopin, C., Goffé, B., 2010. Evolution of the Raman spectrum of carbonaceous material in low grade metasediments of the Glarus Alps (Switzerland). *Terra Nova* 22, 354–360.
- Warr, L.N., 2021. IMA–CNMNC approved mineral symbols. *Mineral. Mag.* 85, 291–320.